World Journal of Radiology

Submit a Manuscript: http://www.wjgnet.com/esps/
Help Desk: http://www.wjgnet.com/esps/helpdesk.aspx
DOI: 10.4329/wjr.v8.i11.857

World J Radiol 2016 November 28; 8(11): 857-867
ISSN 1949-8470 (online)

REVIEW

Diffusion-weighted imaging of the liver: Current applications

Kazuhiro Saito, Yu Tajima, Taiyo L Harada

Kazuhiro Saito, Yu Tajima, Taiyo L Harada, Department of Radiology, Tokyo Medical University, Tokyo 160-0023, Japan

Author contributions: All authors contributed equally to this work; wrote and reviewed the paper.

Conflict-of-interest statement: Authors declare no conflict of interests for this article.

Manuscript source: Invited manuscript

Correspondence to: Kazuhiro Saito, MD, Department of Radiology, Tokyo Medical University, 6-7-1 Nishishinjuku, Shinjuku-ku, Tokyo 160-0023, Japan. saito-k@tokyo-med.ac.jp
Telephone: +81-3-33426111

Received: June 3, 2016
Peer-review started: June 6, 2016
First decision: July 26, 2016
Revised: October 11, 2016
Accepted: October 22, 2016
Article in press: October 23, 2016
Published online: November 28, 2016

Abstract

Diffusion-weighted imaging (DWI) of the liver can be performed using most commercially available machines and is currently accepted in routine sequence. This sequence has some potential as an imaging biomarker for fibrosis, tumor detection/characterization, and following/predicting therapy. To improve reliability including accuracy and reproducibility, researchers have validated this new technique in terms of image acquisition, data sampling, and analysis. The added value of DWI in contrast-enhanced magnetic resonance imaging was established in the detection of malignant liver lesions. However, some limitations remain in terms of lesion characterization and fibrosis detection. Furthermore, the methodologies of image acquisition and data analysis have been inconsistent. Therefore, researchers should make every effort to not only improve accuracy and reproducibility but also standardize imaging parameters.

Key words: Diffusion weighted imaging; Liver; Fibrosis; Lesion characterization

Core tip: The current application of diffusion-weighted imaging (DWI) is reviewed. DWI has some potential as an imaging biomarker for fibrosis, tumor detection/characterization, and following/predicting therapy. However, some limitations remain in terms of lesion characterization and fibrosis detection. To improve reliability including accuracy and reproducibility, researchers have validated this new technique in terms of image acquisition, data sampling, and analysis.

Saito K, Tajima Y, Harada TL. Diffusion-weighted imaging of the liver: Current applications. *World J Radiol* 2016; 8(11): 857-867 Available from: URL: http://www.wjgnet.com/1949-8470/full/v8/i11/857.htm DOI: http://dx.doi.org/10.4329/wjr.v8.i11.857

INTRODUCTION

Diffusion-weighted imaging (DWI) is an imaging method that allows the mapping of the free diffusion of water molecules which reflects the structural differences in

disease by restricting diffusion. DWI can be added to the routine examination easily using recently available machines. This imaging method has a good ability to detect liver lesions, and quantitative evaluation can be achieved without contrast media. Therefore, DWI does not require considerations for patients having contrast media allergy and the risk of nephrogenic systemic fibrosis due to renal dysfunction[1].

FUNDAMENTALS AND TECHNIQUES

Theory

When assuming free water, water molecules spread three-dimensionally with time and temperature dependence by Brownian motion. It is represented by the Einstein-Smoluchowski formula: $<r^2> = 6Dt$, $D = \mu K_B T$, where r is the average distance, D is the diffusion coefficient, *t* is time, μ is mobility, K_B is Boltzmann's constant, and T is the absolute temperature. This spread follows the Gaussian distribution called free diffusion.

Stejskal and Tanner previously measured the diffusion coefficient along with their theory using a binary magnetic field gradient by the spin-echo method[2]. At present, DWI acquisition is commonly performed with a Spin-Echo echo planar imaging (EPI) sequence. Water molecule movement was impeded by the cell membrane, interstitial space, and macromolecules. The movement did not follow the Gaussian probability distribution. When D (diffusion coefficient) is small or time "*t*" is short, the measured D is the same as that of free diffusion because water molecules rarely interact with barrier structures. On the other hand, there is a high probability of the movement being affected by a barrier structure when time "*t*" is greater, which causes the measured D to become smaller than that of free diffusion. This state is referred to as restricted diffusion.

High cellularity, distortion of the extracellular space, and density of the hydrophobic cell membrane within the tissue restrict diffusion. In contrast, an intravoxel microvessel which travels disorderly behaves similarly to a diffusion phenomenon. As mentioned above, DWI enables not only pure diffusion but also microvessel perfusion. Therefore, the diffusion coefficient is designated comprehensively as apparent diffusion coefficient (ADC).

As the *b*-value increases on DWI, the signal decreases in tissues composed chiefly of large diffusion components such as free water owing to phase dispersion, and thus the contrast to tissues that restrict diffusion becomes more clear. *b*-value is defined by the following equation[2]: $b\ (s/mm^2) = -\gamma^2 \cdot G^2 \cdot \delta^2 (\Delta - \delta/3)$, where γ is the gyromagnetic ratio, G is the diffusion gradient amplitude, δ is the gradient diffusion length, and Δ is the diffusion time.

ADC is calculated using the following formula: $S_b/S_0 = \exp(-b \cdot ADC)$, where S_b and S_0 are the signal intensity with and without the application of the diffusion gradient, respectively. This formula is a monoexponential model which does not fit with actual measurement. This is the reason why the signal intensity in the voxel is affected by blood microcirculation. Le Bihan *et al*[3] have proposed the theory of intravoxel incoherent motion (IVIM). They considered blood microcirculation as rapid diffusion, and defined pure molecular diffusion coefficient (D) and pseudodiffusion coefficient (D*). This biexponential model was defined using the following formula when multiple *b*-values are obtained, from low *b*-values (< 200 s/mm^2) to high *b*-values (> 200 s/mm^2): $S_b/S_0 = f \times \exp[-(D^* + D) \times b] + (1 - f) \times (-D \times b)$, where D is the true diffusion coefficient, D* is the pseudodiffusion coefficient, and f is the perfusion fraction. The IVIM model has been applied to the evaluation of liver fibrosis and tumor characterization[4,5]. However, some controversial issues about IVIM have remained. The poor reproducibility of D* has been reported[6,7]. Selection of a fitting model is also crucial for IVIM parameters, because the choice of the *b*-value and reproducibility may be closely related to the fitting models[8].

Advance of technology

DWI using parallel imaging allows for a shorter echo time, and it facilitates improvement of the signal-to-noise (SNR) ratio and thus decreasing susceptibility to artifact[9]. Furthermore, distortion, blurring, and off-resonance artifact diminish, and this increases the spatial resolution[10]. ADC measurement using parallel imaging is reliable except for ADC measurement in the left lobe of the liver[11]. The SNR increases at a high field strength system, but there are some concerns about the inferiority of image quality owing to artifact or signal decay by B0/B1 inhomogeneity, T2/T2* shortening, and increasing acoustic gradient noise. However, using parallel imaging offsets these disadvantages[12].

Single shot EPI sequence is sensitized to not only the motion of diffusion but also bulk motion. Therefore, the consideration of respiration and pulsation is important in case of the acquisition of liver images. In image acquisition during breath holding, it is unnecessary to consider respiratory artifact, in contrast to some disadvantages such as low spatial resolution, low SNR, distortion, and ghost artifact. On the other hand, the free breathing (FB) method usually takes a few minutes because of the many acquisition times, and as a result the SNR increases. Moreover, a high spatial resolution can be achieved and thin slices can be obtained[13]. However, the disadvantage of the FB method is that it is less reliable if there is heterogeneity in the lesion owing to the averaging and blurring of the image. The navigator-triggered (NT) acquisition is a method for running the image sequence in accordance with the expiratory phase monitoring the movement of the diaphragm on high-speed imaging systems such as FLASH during FB. The NT technique improves image quality and lesion contrast, and increases SNR. Moreover, it enables accurate ADC measurement[14,15]. Artifact also becomes stronger as *b*-value increases[15]. In addition, a specific artifact reported as hepatic pseudoanisotropy attributed to performing DWI

in the respiratory gating (RT) has been reported[16].

ADC was reported to be affected by SNR, susceptibility artifact, or artifact derived from heart beating or liver motion due to respiration. Although FB tends to scatter signals compared with RT, the ADC does not differ[17]. The SNR on RT is higher than that on BH. The ADC is also slightly higher on RT than on BH[14]. In a comparison between NT and FB, both are reportedly similar in terms of the ADC and IVIM parameters[18].

For ADC reproducibility, RT is superior to BH but inferior to FB in healthy liver parenchyma[19]. Similarly, in a comparison study among multiple breath-hold (MBH), FB, RT, and NT, FB showed the best ADC reproducibility[20]. It should be noted that there were differences in the signal acquisition times among those techniques in these comparison studies[20].

Effects of contrast agent administration

Currently, Gd-EOB-DTPA-enhanced MRI has been widely used for the detection of liver lesions. However, it is necessary to wait for about 20 min for optimal liver parenchymal enhancement[21]. To improve the examination throughput, DWI is undertaken after Gd-EOB-DTPA injection. Gd-EOB-DTPA does not have an effect on ADC[22]. Furthermore, considering the biexponential IVIM model, there were also no effects on D, D*, and PF[23]. Based on these facts, even if DWI is not successful prior to contrast administration, the lesion can be evaluated on the images acquired during the waiting time until the hepatobiliary phase.

Weak feature of DWI

Cardiac motion causes negligible artifact (signal loss) on DWI of the liver. This artifact tends to become emphasized with a higher *b*-value and is closer to the heart. Thus, the artifact in the left lobe around the lower surface of the heart in particular can make an image particularly obscure[19,24]. The liver-to-background contrast is also changed by the cardiac phase of acquisition; it decreases more at the systolic phase and signal loss is larger in the left lobe[25]. The ADC of the left lobe is higher and its reproducibility is worse compared with the right lobe[26]. Some solutions to reduce the effects of cardiac motion have been proposed. These include the postprocessing method[24] or filtering[27] which corrects the image after signal acquisition or cardiac triggering synchronized with the heart cycle[27,28]. ADC reproducibility was reportedly improved using these methods.

Moreover, susceptibility artifact occurs at the boundary surfaces between the lungs and the liver parenchyma because of magnetic field inhomogeneity[29]. The artifact is observed as a signal loss in the diaphragm or liver.

Peristaltic movement can produce ghost artifact or blurring on abdominal MRI in the pancreas and liver near the intestinal tract[30]. Hyoscine butylbromide suppresses contraction of the smooth muscles in the intestines and it can reduce ghost artifact (peristaltic artifact). Moreover, it can similarly improve the image quality[31]. As hyoscine butylbromide administration can increase the heart rate, it has also been pointed out that the image quality of the subcardiac area in the hepatic left lobe is reduced on visual evaluation. However, there is no observed significant change in ADC[32]. Thus, it is necessary to address all of the challenges associated with DWI of the liver to achieve higher levels of quantitative and qualitative outcomes and to obtain precise assessments.

EVALUATION OF LIVER FIBROSIS

Clinical application

Liver fibrosis is the accumulation of scar tissue resulting from hepatocyte response to chronic inflammation caused by the hepatitis B or C virus and alcohol consumption, among many other causes[33]. Chronic inflammation activates the stellate cells and induces fibrosis of the extracellular matrix (ECM). In this process, molecules such as glycogen, proteoglycan, and other macromolecules accumulate in the ECM, restricting ECM diffusion[34,35]. Fibrosis leads to cirrhosis, portal hypertension after many years, and possibly eventual death. Liver biopsy is a widely accepted procedure for diagnosing and grading liver fibrosis. However, this procedure is associated with major complications in 0.3% and with mortality in 0.018% of patients[36]. Furthermore, because of the heterogeneity of liver fibrosis, sampling errors can also arise[37,38]. Therefore, alternative noninvasive diagnostic methods that can precisely evaluate liver fibrosis are desirable. Because of convenience and repeatability, the usefulness of some diffusion-weighted MRI parameters (*e.g.,* ADC) and IVIM parameters has been evaluated in several studies. DWI enables the evaluation of restricted diffusion caused by collagen fibers accumulated in the ECM in cirrhotic liver[39-41]. In relation to this, it is important to distinguish METAVIR fibrosis stage 3 or 4 from stages 0 to 2 because patients in the F0-2 grades can be cured by treating the underlying liver disease[42].

Evaluating liver fibrosis using ADC

Several studies have shown that ADC decreases as the liver fibrosis grade progresses[40,41,43,44]. Specifically, the diagnostic performance of detecting METAVIR fibrosis grade 3 or 4 was variable and the area under the ROC curve (AUC) was 0.54-0.92. Some studies have concluded that MR elastography was more reliable than DWI[44,45]. Do *et al*[46] proposed normalized ADC to improve the diagnostic accuracy of DWI. They calculated normalized ADC as the ratio of liver ADC to spleen ADC and reported that the AUC increased from 0.689 to 0.805 using their methods (Table 1).

Evaluating liver fibrosis using IVIM parameters

The efficacy of diagnosing liver fibrosis has been reported by Luciani *et al*[5]. They found that perfusion-related diffusion parameters (D*: Fast component of diffusion, f: Fraction of the diffusion linked to microcirculation) were

Table 1 Detection of fibrosis using diffusion-weighted imaging

	Tesla	Respiratory	Staging	ROI setting	*b*-value	Diagnostic accuracy of fibrosis F3 or grater		
						AUC	Sensitivity	Specificity
Cece *et al*[91]	1.5	BH	MTAVIR	5 ROIs, Both	0, 500, 1000	0.888	92.9	79.4
Taouli *et al*[92]	1.5	BH	MTAVIR	4 ROIs, Both	0, 50	0.717	40	100
					0, 300	0.716	50	94.7
					0, 500	0.835	70	85
					0, 700	0.901	66.7	100
					0, 1000	0.832	80	90
					0, 50, 300, 500, 700, 1000	0.896	88.9	80
Kocakoc *et al*[93]	1.5	BH	Ishak	3 ROIs, Both	100, 600, 1000	0.759	56.5	99.3
Wu *et al*[47]	3	RT	MTAVIR	5 ROIs, Right	0, 10, 20, 30, 40, 50, 60, 70, 80, 90, 100, 200, 300, 400, 500, 1000	0.684		
Chung *et al*[48]	1.5	RT	MTAVIR	6 ROIs, Right	0, 100, 200, 900	0.768		
					0, 30, 60, 100, 150, 200, 900	0.764		
					0, 30, 60, 100, 150, 200, 400, 600, 900	0.754	65.5	82.1
Ding *et al*[94]	1.5	FB	New Inuyama	Whole right lobe	0, 500	0.61	30.4	90.6
Feier *et al*[43]	3	NA	MTAVIR	1 ROI, Right	50, 300, 600	0.77	81.08	72.5
Fujimoto *et al*[95]	1.5	NA	MTAVIR	4 ROIs, Right	0, 1000 (entropy ADC)	0.926	87	84
Do *et al*[46]	1.5	BT	Ludwig	4 ROIs, Right	0, 50, 500 (normalized ADC)	0.689	56	71
Bonekamp *et al*[96]	1.5	BT	MTAVIR	9 ROIs, Both	0, 750	0.8	83.9	68.5
Wang *et al*[44]	1.5	NA	MTAVIR	3 ROIs, Right	50, 500, 1000	0.84	88	76
Lewin *et al*[41]	1.5	RT	MTAVIR	3 ROIs, Right	0, 200, 400, 800	0.92	87	87
Sandrosegaran *et al*[40]	1.5	BH		2 ROIs, Both	50, 400	0.656	51.7	71.4

BH: Breath-hold; RT: Respiratory gating.

significantly related to restricted diffusion in a cirrhotic liver, whereas diffusion-related parameters (D: Slow component of diffusion) were not significantly related. Several studies followed after this study[5,45,47-53]. Including the study of Luciani *et al*[5], 3 studies[49,52,53] only compared cirrhotic liver with healthy volunteer liver but did not evaluate the fibrosis grade. D* was found to be significantly lower in the cirrhotic liver in all studies and D showed a significantly lower value in 2 studies[52,53]. In these 2 studies, the authors adopted relatively more of high *b*-values and less of low *b*-values. On the other hand, Chung *et al*[48] calculated IVIM parameters using 3 patterns of *b*-value selection to diagnose high-grade liver fibrosis: b = 0, 30, 60, 100, 150, 200, 400, 600, 900 s/mm^2; b = 0, 30, 60, 100, 150, 200, 900 s/mm^2; and b = 0, 100, 200, 900 s/mm^2. They suggested that the number of lower *b*-values was not crucial for diagnosing high-grade liver fibrosis. Girometti *et al*[50] have suggested that higher *b*-values may not be necessary for diagnosing liver fibrosis. Supporting these hypotheses, Wu *et al*[47] suggested that favorable results were given by *b*-values 0, 20, 40, 60, 80, 100, 150, 200, 400, and 800 s/mm^2.

Effects of steatosis

Steatosis has been reported to have possible effects on ADC. Poyraz *et al* have suggested that steatosis decreases ADC because the increased fat content of hepatocytes and the extracellular fat accumulation reduce the interstitial space and restrict water diffusion[39,54]. Other studies have evaluated the effects of fat deposition by DWI using other methods. These studies estimated that fat has several components that broaden the spectrum and mimic T2* decay at short TE ranges; however, the accurate mechanism is unknown[55,56]. Another study mentioned that IVIM parameters, such as diffusion coefficient and perfusion fraction, are not affected by the fat fraction and have the possibility of evaluating liver fibrosis regardless of the fat deposition[57].

Effects of iron deposition

The most widely used sequence for DWI is EPI, which allows acquisition of a full slice in a single shot. However, the EPI readout is also subject to ghosting and susceptibility artifacts, and may decrease ADC as a result of the T2* shortening effect[8,58]. Chronic liver disease may often have iron overload. Therefore, if extremely low ADCs are obtained, iron overload should be considered[59-63].

DETECTION AND CHARACTERIZATION OF LIVER TUMORS

Detection of liver tumors

DWI has a better contrast-to-noise ratio and better conspicuity by suppression of background vessels in low *b*-values[64]. DWI has a higher detection rate of liver tumors than T2WI[64,65], particularly in detecting malignant lesions[66]. However, the ADC of benign solid lesions has been reported to be similar to that of the liver parenchyma[67]. Therefore, benign solid lesions may be difficult to detect on DWI.

Many studies have reported that DWI has an additional value for detecting liver metastasis in combination with Gd-EOB-DTPA (Table 2); however, this remains controversial in hepatocellular carcinoma (HCC). Some

Table 2 Detection of liver tumor in combination with Gd-EOB-DTPA- enhanced magnetic resonance imaging

	Tesla	Respiratory	*b*-value ($\times 10^{-3}$ s/mm^2)	Tumor	Results
Kim *et al*[97]	3	RT	0, 100, 800	Mets (Various)	Combined EOB-MRI and DWI yielded better accuracy and sensitivity
Chung *et al*[98]	3	FB	50, 400, 800	Mets (colorectal)	Combined EOB-MRI and DWI yielded better accuracy and sensitivity
Koh *et al*[99]	1.5	FB	0, 50, 100, 250, 500, 750	Mets (colorectal)	Combined EOB-MRI and DWI improved detection
Löwenthal *et al*[100]	1.5	BH	0, 500	Mets (colorectal)	DWI can detect small lesions
Shimada *et al*[101]	3	RT	0, 500	Mets (Various)	EOB-MRI showed higher accuracy
Donati *et al*[102]	1.5	BH	0, 150, 500	Mets (Various)	No added value of DWI
Kim *et al*[103]	1.5	RT	0, 50, 600	Mets, HCC	DWI increases sensitivity for detecting Mets No added value of DWI for HCC detection

DWI: Diffusion-weighted imaging; BH: Breath-hold; RT: Respiratory gating; FB: Free breathing; HCC: Hepatocellular carcinoma.

Table 3 Characteristic differentiation of liver tumors

	Tesla	*b*-value	ADC ($\times 10^{-3}$ mm^2)					
			Benign			Malignant		
			Cyst	Hemangioma	All	HCC	Mets	All
Goshima *et al*[104]	1.5	0, 100, 200, 400, 800	3.70 ± 0.9	1.23 ± 0.2		1.08 ± 0.3	0.99 ± 0.5	
Battal *et al*[105]	1.5	0, 800			1.94 ± 0.61			0.86 ± 0.13
Gurtosoyianni *et al*[106]	1.5	0, 50, 500, 1000	2.55	1.9	2.55	1.38	0.99	1.04
Testa *et al*[71]	1.5	0, 600	2.4				1	
Miller *et al*[73]	1.5	0, 500	3.40 ± 0.48	2.26 ± 0.70	2.50 ± 0.86	1.54 ± 0.44	1.50 ± 0.65	1.52 ± 0.55
Namimoto *et al*[107]	1.5	30, 1200	3.05	1.95		0.99	1.15	1.04
Kim *et al*[108]	1.5	3, 57, 192, 408, 517, 705, 846	2.91 ± 1.51	2.04 ± 1.01	2.49 ± 1.39	0.97 ± 0.31	1.06 ± 0.50	1.01 ± 0.38
Taouli *et al*[67]	1.5	0, 500	3.63 ± 0.56	2.95 ± 0.67		1.33 ± 0.13	0.94 ± 0.60	
Cieszanowsk *et al*[109]	1.5	50, 400, 800	2.45	1,55	1.86	0.94	1.05	1.07
Bruegel *et al*[72]	1.5	50, 300, 600	3.02 ± 0.31	1.92 ± 0.34		1.05 ± 0.09	1.22 ± 0.31	
Kandpal *et al*[13]	1.5	0, 500	2.90 ± 0.51	2.36 ± 0.48		1.27 ± 0.42	1.13 ± 0.41	
Demir *et al*[110]	1.5	0, 1000	3.05 ± 0.26	2.46 ± 0.21	2.57 ± 0.26	0.90 ± 0.10	0.79 ± 0.11	0.86 ± 0.11
Oner *et al*[111]	1.5	0, 500	2.34 ± 0.36	1.72 ± 0.30			1.03 ± 0.24	
Holzapfel *et al*[112]	1.5	50, 300, 600	2.61 ± 0.57	1.69 ± 0.34	2.36 ± 0.62	1.12 ± 0.28	1.08 ± 0.32	1.09 ± 0.30

ADC: Apparent diffusion coefficient; HCC: Hepatocellular carcinoma.

authors have reported no additional value because some well-differentiated HCCs could not be detected on DWI as the major reason[68]. Well-differentiated HCCs include variable pathological characteristics like as early HCCs whose pathology is very similar to the surrounding liver parenchyma, steatosis contained lesion and a hypervascular lesion. Kim *et al*[69] reported that early HCCs showed hyperintensity on DWI which was strongly associated with their progression to hypervascular HCCs.

Characteristic differentiation of liver tumors (benign vs malignant)

In hypercellular tissue, extracellular water cannot diffuse and this results in a reduction in ADC. A cystic component has few structures to restrict diffusion and this result in a high ADC. Cysts can be distinguished from solid lesions easily. The cut-off ADC was reported to be approximately 2.5 × 10^{-3} mm^2/s for distinguishing cysts from other solid liver tumors[70]. Hemangioma is also relatively easy to distinguish from malignant lesions. The ADC of hemangioma was reported to be approximately 1.4 × 10^{-3} mm^2/s. However, some overlaps have been recognized which reduce accuracy in distinguishing metastatic lesions[71]. This is particularly true for mucinous carcinoma from the ovary which mimics colorectal carcinoma (Figure 1). However, tumor characterization was reportedly not dependent on size[72] (Table 3).

DWI is reportedly not helpful in differentiating focal nodular hyperplasia and adenoma from solid malignant lesions. The mean ADCs of these benign solid lesions were reported as 1.40-1.79 × 10^{-3} mm^2/s[72,73]. Notably, the ADCs of these benign solid lesions and those of malignant lesions such as HCCs and metastatic tumors overlap (Figure 2).

Histological differentiation of HCC

Preoperative prediction of the histological grade of HCC

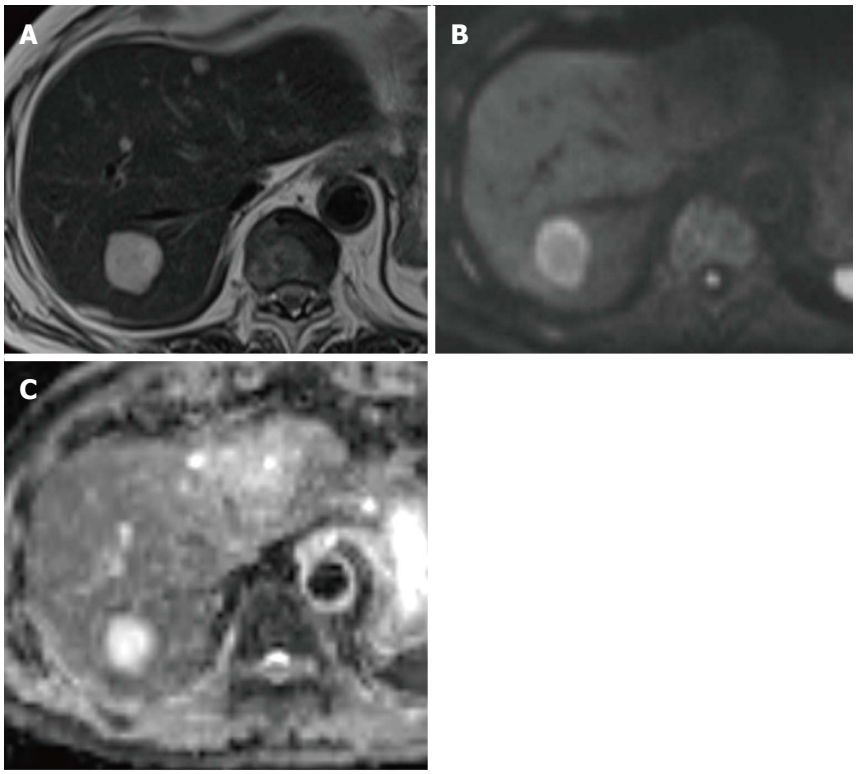

Figure 1 A 65-year-old man with metastatic tumor in the liver from colorectal carcinoma. A: T2-weighted imaging shows an obvious hyperintense lesion on segment VII (arrow); B: DWI (*b*-value of 800 s/mm^2) shows hyperintensity; C: Apparent diffusion coefficient map also shows hyperintensity. This finding mimics that for hemangioma. DWI: Diffusion-weighted imaging.

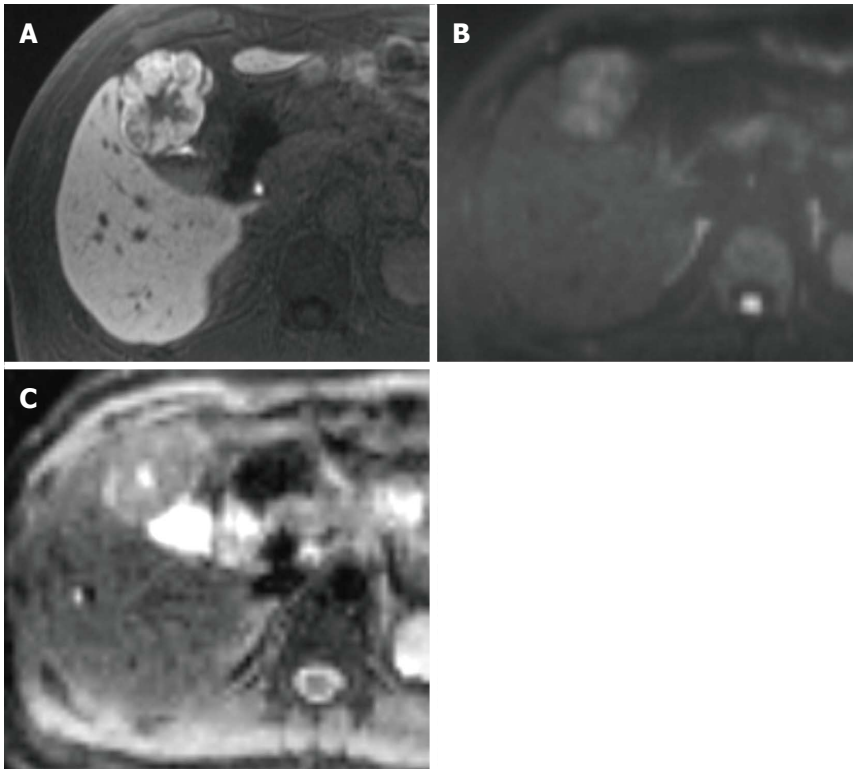

Figure 2 A 45-year-old man with focal nodular hyperplasia. A: Hepatobiliary phase on Gd-EOB-DTPA-enhanced MRI shows mainly hyperintensity on the outer layer and hypointensity on the inner layer. These enhancement patterns are typical radiologic findings of focal nodular hyperplasia; B: DWI (*b*-value of 800 s/mm^2) shows hyperintensity; C: ADC map shows heterogeneous hyperintensity. The ADC is 1.40 × 10^{-3} mm^2/s. Gd-EOB-DTPA-enhanced MRI is more useful for obtaining a precise diagnosis than DWI alone. MRI: Magnetic resonance imaging; DWI: Diffusion-weighted imaging; ADC: Apparent diffusion coefficient.

can facilitate the estimation of prognosis and contribute to the choice of therapy. There is also a higher incidence of recurrence in poorly differentiated HCCs than in well-differentiated and moderately differentiated HCCs[74,75].

Histological grade correlates with cellularity and structural atypia which includes trabecular, pseudoglandular, solid, and scirrhus. As HCC progresses to poorly differentiated HCC, there is increased cellular density, nuclear/cytoplasmic ratio and intracellular organelles; thickened cellular plates; and shrinkage of the extracellular and intracellular spaces. This may lead to restricted diffusion in poorly differentiated HCC. However, the results have been inconsistent[75-79] (Table 4). One of the main reasons for this inconsistency is the region of interest (ROI) setting. Previous studies showed no significant differences in the ROI setting for each histological grade on whole lesions[76,77]. On the

Table 4 Histological differentiation of hepatocellular carcinoma using apparent diffusion coefficient

	Tesla	Respiratory	*b*-value (s/mm^2)	Well-diff HCC ($\times 10^{-3}$ mm^2/s)	Mod diff HCC ($\times 10^{-3}$ mm^2/s)	Poorly diff HCC ($\times 10^{-3}$ mm^2/s)	Difference
Saito *et al*[113]	1.5	RT	100, 800	1.25 ± 0.25	1.12 ± 0.22	1.13 ± 0.23	NS
Nasu *et al*[114]	1.5	RT	0, 500	1.45 ± 0.35	1.46 ± 0.32	1.36 ± 0.29	NS
Heo *et al*[77]	1.5	FB	0, 1000	1.2 ± 0.22	1.1 ± 0.10	0.9 ± 0.13	p < w, m
Nakanishi *et al*[80]	1.5	RT	50, 1000	NA	1.29 ± 0.21	1.07 ± 0.15	p < m
Nishie *et al*[75]	1.5	RT	0, 500, 1000	1.21 ± 0.11	1.14 ± 0.26	0.76 ± 0.10	p < w, m
Guo *et al*[79]	3.0	BH	0, 600	1.43 ± 0.09	1.34 ± 0.19	1.16 ± 0.16	p < w, m

RT: Respiratory trigger; BH: Breath holding; FB: Free breathing; ADC: Apparent diffusion coefficient. p < w, m: ADC in poorly differentiated HCC was significantly lower than ADC in well-differentiated HCC and moderately differentiated HCC; p < m: ADC in poorly differentiated HCC was significantly lower than ADC in moderately differentiated HCC; NS: No significant difference in ADC was observed for each histological grade; NA: Not applicable.

other hand, in cases of the ROI set at the lowest ADC and the ROI set to avoid a necrotic or cystic area, a lower ADC was obtained in poorly differentiated HCC[75,78,79].

The current applications are IVIM and ADC minimum. D shows a better diagnostic performance than ADC in distinguishing high-grade HCC from low-grade HCC[80]. ADC contains combined information on cell density (D) and perfusion (f) (microcirculation). Minimum-spot ADC was reported to be significantly lower in poorly differentiated HCC than in well-differentiated HCC and moderately differentiated HCC[75].

MONITORING OF THERAPY

Transarterial chemoembolization in HCC

Tumor necrosis shows a high intensity on the ADC map, representing free diffusion of water molecules[81]. Therefore, DWI can evaluate the therapeutic outcome of transarterial chemoembolization (TACE). In case of a hypervascular lesion without a definite venous washout, DWI has an advantage compared with dynamic MRI and improves the detection of marginal tumor recurrence[14], although dynamic MRI has a more accurate correlation with histopathological findings in necrosis. TACE-induced perilesional parenchymal changes negatively affect DWI in terms of overall accuracy. On the other hand, Kokabi *et al*[82] reported that an ADC change 3 h after TACE is an accurate predictor of treatment response and survival.

IVIM and diffusion kurtosis imaging (DKI) are current imaging biomarkers. Specifically, D* predicts lipiodol uptake[83]. DKI is reportedly a more reliable imaging biomarker than ADC[84].

Chemotherapy in liver metastasis

Some studies have reported that ADC could predict the response to chemotherapy in liver metastasis[85,86]. Liang *et al* reported that pretreatment ADC is significantly lower in responders[87]. In contrast, Koh *et al*[85] reported that a high pretreatment ADC predicted a poor response. Furthermore, ADC increases 3 or 7 d after chemotherapy in responders. Recently, ADC histogram analysis has shown that the mean, 1st percentile, 10th percentile, 50th percentile, 90th percentile, and 99th percentile were significantly lower in the responding group than in the nonresponding group. The reason why ADC in responders is lower is that high cell density tumors are well perfused, resulting in the high delivery and retention of chemotherapeutic drugs.

Sorafenib in HCC

IVIM has been proposed for evaluating the therapeutic outcome of sorafenib[88,89]. D before treatment in responders was found to be higher than D before treatment in nonresponders[88]. This might be due to the tumor histological grade. Sorafenib acts more effectively in low-grade HCCs[90]. D can better distinguish low-grade HCCs from high-grade HCCs[80], and a higher D indicates low-grade HCCs. Lewin *et al*[89] reported that f increased significantly in responders after 2 wk. This perfusion parameter f increases with normalization of tumor vessels.

CONCLUSION

DWI has potential as an imaging biomarker for fibrosis, tumor detection/characterization, and following/predicting therapy outcome. To improve accuracy and reproducibility, researchers have validated this new technique in terms of image acquisition, data sampling, and analysis. The added value of DWI in contrast-enhanced MRI has been established in the detection of malignant lesions of the liver. However, some limitations remain in terms of lesion characterization and fibrosis detection. Furthermore, the methodologies of image acquisition and data analysis have been inconsistent. Therefore, researchers should make every effort not only to improve accuracy and reproducibility but also to standardize the imaging parameters.

REFERENCES

1 **Prince MR**, Zhang H, Zou Z, Staron RB, Brill PW. Incidence of immediate gadolinium contrast media reactions. *AJR Am J Roentgenol* 2011; **196**: W138-W143 [PMID: 21257854 DOI: 10.2214/AJR.10.4885]

2 **Stejskal EO**, Tanner JE. Spin diffusion measurements: spin echoes in the presence of a time-dependent field gradient. *J Chem Phys* 1965; **42**: 288-292 [DOI: 10.1063/1.1695690]

3 **Le Bihan D**, Breton E, Lallemand D, Grenier P, Cabanis E, Laval-Jeantet M. MR imaging of intravoxel incoherent motions: application to diffusion and perfusion in neurologic disorders.

Radiology 1986; **161**: 401-407 [PMID: 3763909 DOI: 10.1148/radiology.161.2.3763909]
4 **Yamada I**, Aung W, Himeno Y, Nakagawa T, Shibuya H. Diffusion coefficients in abdominal organs and hepatic lesions: evaluation with intravoxel incoherent motion echo-planar MR imaging. *Radiology* 1999; **210**: 617-623 [PMID: 10207458 DOI: 10.1148/radiology.210.3.r99fe17617]
5 **Luciani A**, Vignaud A, Cavet M, Nhieu JT, Mallat A, Ruel L, Laurent A, Deux JF, Brugieres P, Rahmouni A. Liver cirrhosis: intravoxel incoherent motion MR imaging--pilot study. *Radiology* 2008; **249**: 891-899 [PMID: 19011186 DOI: 10.1148/radiol.2493080080]
6 **Andreou A**, Koh DM, Collins DJ, Blackledge M, Wallace T, Leach MO, Orton MR. Measurement reproducibility of perfusion fraction and pseudodiffusion coefficient derived by intravoxel incoherent motion diffusion-weighted MR imaging in normal liver and metastases. *Eur Radiol* 2013; **23**: 428-434 [PMID: 23052642 DOI: 10.1007/s00330-012-2604-1]
7 **Dyvorne HA**, Galea N, Nevers T, Fiel MI, Carpenter D, Wong E, Orton M, de Oliveira A, Feiweier T, Vachon ML, Babb JS, Taouli B. Diffusion-weighted imaging of the liver with multiple b values: effect of diffusion gradient polarity and breathing acquisition on image quality and intravoxel incoherent motion parameters--a pilot study. *Radiology* 2013; **266**: 920-929 [PMID: 23220895 DOI: 10.1148/radiol.12120686]
8 **Chandarana H**, Do RK, Mussi TC, Jensen JH, Hajdu CH, Babb JS, Taouli B. The effect of liver iron deposition on hepatic apparent diffusion coefficient values in cirrhosis. *AJR Am J Roentgenol* 2012; **199**: 803-808 [PMID: 22997371 DOI: 10.2214/AJR.11.7541]
9 **Taouli B**, Martin AJ, Qayyum A, Merriman RB, Vigneron D, Yeh BM, Coakley FV. Parallel imaging and diffusion tensor imaging for diffusion-weighted MRI of the liver: preliminary experience in healthy volunteers. *AJR Am J Roentgenol* 2004; **183**: 677-680 [PMID: 15333355 DOI: 10.2214/ajr.183.3.1830677]
10 **Bammer R**, Keeling SL, Augustin M, Pruessmann KP, Wolf R, Stollberger R, Hartung HP, Fazekas F. Improved diffusion-weighted single-shot echo-planar imaging (EPI) in stroke using sensitivity encoding (SENSE). *Magn Reson Med* 2001; **46**: 548-554 [PMID: 11550248 DOI: 10.1002/mrm.1226]
11 **Yoshikawa T**, Kawamitsu H, Mitchell DG, Ohno Y, Ku Y, Seo Y, Fujii M, Sugimura K. ADC measurement of abdominal organs and lesions using parallel imaging technique. *AJR Am J Roentgenol* 2006; **187**: 1521-1530 [PMID: 17114546 DOI: 10.2214/AJR.05.0778]
12 **Wiesinger F**, Van de Moortele PF, Adriany G, De Zanche N, Ugurbil K, Pruessmann KP. Parallel imaging performance as a function of field strength--an experimental investigation using electrodynamic scaling. *Magn Reson Med* 2004; **52**: 953-964 [PMID: 15508167 DOI: 10.1002/mrm.20281]
13 **Kandpal H**, Sharma R, Madhusudhan KS, Kapoor KS. Respiratory-triggered versus breath-hold diffusion-weighted MRI of liver lesions: comparison of image quality and apparent diffusion coefficient values. *AJR Am J Roentgenol* 2009; **192**: 915-922 [PMID: 19304695 DOI: 10.2214/AJR.08.1260]
14 **Taouli B**, Sandberg A, Stemmer A, Parikh T, Wong S, Xu J, Lee VS. Diffusion-weighted imaging of the liver: comparison of navigator triggered and breathhold acquisitions. *J Magn Reson Imaging* 2009; **30**: 561-568 [PMID: 19711402 DOI: 10.1002/jmri.21876]
15 **Asbach P**, Hein PA, Stemmer A, Wagner M, Huppertz A, Hamm B, Taupitz M, Klessen C. Free-breathing echo-planar imaging based diffusion-weighted magnetic resonance imaging of the liver with prospective acquisition correction. *J Comput Assist Tomogr* 2008; **32**: 372-378 [PMID: 18520540 DOI: 10.1097/RCT.0b013e3180dc930c]
16 **Nasu K**, Kuroki Y, Fujii H, Minami M. Hepatic pseudo-anisotropy: a specific artifact in hepatic diffusion-weighted images obtained with respiratory triggering. *MAGMA* 2007; **20**: 205-211 [PMID: 17960439 DOI: 10.1007/s10334-007-0084-0]
17 **Nasu K**, Kuroki Y, Sekiguchi R, Nawano S. The effect of simultaneous use of respiratory triggering in diffusion-weighted imaging of the liver. *Magn Reson Med Sci* 2006; **5**: 129-136 [PMID: 17139138 DOI: 10.2463/mrms.5.129]
18 **Jerome NP**, Orton MR, d'Arcy JA, Collins DJ, Koh DM, Leach MO. Comparison of free-breathing with navigator-controlled acquisition regimes in abdominal diffusion-weighted magnetic resonance images: Effect on ADC and IVIM statistics. *J Magn Reson Imaging* 2014; **39**: 235-240 [PMID: 23580454 DOI: 10.1002/jmri.24140]
19 **Kwee TC**, Takahara T, Koh DM, Nievelstein RA, Luijten PR. Comparison and reproducibility of ADC measurements in breathhold, respiratory triggered, and free-breathing diffusion-weighted MR imaging of the liver. *J Magn Reson Imaging* 2008; **28**: 1141-1148 [PMID: 18972355 DOI: 10.1002/jmri.21569]
20 **Chen X**, Qin L, Pan D, Huang Y, Yan L, Wang G, Liu Y, Liang C, Liu Z. Liver diffusion-weighted MR imaging: reproducibility comparison of ADC measurements obtained with multiple breath-hold, free-breathing, respiratory-triggered, and navigator-triggered techniques. *Radiology* 2014; **271**: 113-125 [PMID: 24475860 DOI: 10.1148/radiol.13131572]
21 **Hamm B**, Staks T, Mühler A, Bollow M, Taupitz M, Frenzel T, Wolf KJ, Weinmann HJ, Lange L. Phase I clinical evaluation of Gd-EOB-DTPA as a hepatobiliary MR contrast agent: safety, pharmacokinetics, and MR imaging. *Radiology* 1995; **195**: 785-792 [PMID: 7754011 DOI: 10.1148/radiology.195.3.7754011]
22 **Saito K**, Araki Y, Park J, Metoki R, Katsuyama H, Nishio R, Kakizaki D, Moriyasu F, Tokuuye K. Effect of Gd-EOB-DTPA on T2-weighted and diffusion-weighted images for the diagnosis of hepatocellular carcinoma. *J Magn Reson Imaging* 2010; **32**: 229-234 [PMID: 20578029 DOI: 10.1002/jmri.22219]
23 **Colagrande S**, Mazzoni LN, Mazzoni E, Pradella S. Effects of gadoxetic acid on quantitative diffusion-weighted imaging of the liver. *J Magn Reson Imaging* 2013; **38**: 365-370 [PMID: 23239165 DOI: 10.1002/jmri.23978]
24 **Liau J**, Lee J, Schroeder ME, Sirlin CB, Bydder M. Cardiac motion in diffusion-weighted MRI of the liver: artifact and a method of correction. *J Magn Reson Imaging* 2012; **35**: 318-327 [PMID: 21959926 DOI: 10.1002/jmri.22816]
25 **Kwee TC**, Takahara T, Niwa T, Ivancevic MK, Herigault G, Van Cauteren M, Luijten PR. Influence of cardiac motion on diffusion-weighted magnetic resonance imaging of the liver. *MAGMA* 2009; **22**: 319-325 [PMID: 19727877 DOI: 10.1007/s10334-009-0183-1]
26 **Kim SY**, Lee SS, Byun JH, Park SH, Kim JK, Park B, Kim N, Lee MG. Malignant hepatic tumors: short-term reproducibility of apparent diffusion coefficients with breath-hold and respiratory-triggered diffusion-weighted MR imaging. *Radiology* 2010; **255**: 815-823 [PMID: 20501719 DOI: 10.1148/radiol.10091706]
27 **Metens T**, Absil J, Denolin V, Bali MA, Matos C. Liver apparent diffusion coefficient repeatability with individually predetermined optimal cardiac timing and artifact elimination by signal filtering. *J Magn Reson Imaging* 2016; **43**: 1100-1110 [PMID: 26566777 DOI: 10.1002/jmri.25089]
28 **Mürtz P**, Flacke S, Träber F, van den Brink JS, Gieseke J, Schild HH. Abdomen: diffusion-weighted MR imaging with pulse-triggered single-shot sequences. *Radiology* 2002; **224**: 258-264 [PMID: 12091693 DOI: 10.1148/radiol.2241011117]
29 **Atalay MK**, Poncelet BP, Kantor HL, Brady TJ, Weisskoff RM. Cardiac susceptibility artifacts arising from the heart-lung interface. *Magn Reson Med* 2001; **45**: 341-345 [PMID: 11180442]
30 **Wood ML**, Runge VM, Henkelman RM. Overcoming motion in abdominal MR imaging. *AJR Am J Roentgenol* 1988; **150**: 513-522 [PMID: 3257601 DOI: 10.2214/ajr.150.3.513]
31 **Wagner M**, Klessen C, Rief M, Elgeti T, Taupitz M, Hamm B, Asbach P. High-resolution T2-weighted abdominal magnetic resonance imaging using respiratory triggering: impact of butylscopolamine on image quality. *Acta Radiol* 2008; **49**: 376-382 [PMID: 18415778 DOI: 10.1080/02841850801894806]
32 **Nasu K**, Kuroki Y, Sekiguchi R, Kazama T, Nakajima H. Measurement of the apparent diffusion coefficient in the liver: is it a reliable index for hepatic disease diagnosis? *Radiat Med* 2006; **24**: 438-444 [PMID: 16958425 DOI: 10.1007/s11604-006-0053-y]
33 **Friedman SL**. Seminars in medicine of the Beth Israel Hospital, Boston. The cellular basis of hepatic fibrosis. Mechanisms and treatment strategies. *N Engl J Med* 1993; **328**: 1828-1835 [PMID: 8502273 DOI: 10.1056/NEJM199306243282508]

34 **Rojkind M**, Giambrone MA, Biempica L. Collagen types in normal and cirrhotic liver. *Gastroenterology* 1979; **76**: 710-719 [PMID: 421999]

35 **Gressner AM**. The cell biology of liver fibrogenesis - an imbalance of proliferation, growth arrest and apoptosis of myofibroblasts. *Cell Tissue Res* 1998; **292**: 447-452 [PMID: 9582401 DOI: 10.1007/s004410051073]

36 **Wong JB**, Bennett WG, Koff RS, Pauker SG. Pretreatment evaluation of chronic hepatitis C: risks, benefits, and costs. *JAMA* 1998; **280**: 2088-2093 [PMID: 9875876 DOI: 10.1001/jama.280.24.2088]

37 **Regev A**, Berho M, Jeffers LJ, Milikowski C, Molina EG, Pyrsopoulos NT, Feng ZZ, Reddy KR, Schiff ER. Sampling error and intraobserver variation in liver biopsy in patients with chronic HCV infection. *Am J Gastroenterol* 2002; **97**: 2614-2618 [PMID: 12385448 DOI: 10.1111/j.1572-0241.2002.06038.x]

38 **Howlett DC**, Drinkwater KJ, Lawrence D, Barter S, Nicholson T. Findings of the UK national audit evaluating image-guided or image-assisted liver biopsy. Part II. Minor and major complications and procedure-related mortality. *Radiology* 2013; **266**: 226-235 [PMID: 23143026 DOI: 10.1148/radiol.12120224]

39 **Bakan AA**, Inci E, Bakan S, Gokturk S, Cimilli T. Utility of diffusion-weighted imaging in the evaluation of liver fibrosis. *Eur Radiol* 2012; **22**: 682-687 [PMID: 21984447 DOI: 10.1007/s00330-011-2295-z]

40 **Sandrasegaran K**, Akisik FM, Lin C, Tahir B, Rajan J, Saxena R, Aisen AM. Value of diffusion-weighted MRI for assessing liver fibrosis and cirrhosis. *AJR Am J Roentgenol* 2009; **193**: 1556-1560 [PMID: 19933647 DOI: 10.2214/AJR.09.2436]

41 **Lewin M**, Poujol-Robert A, Boëlle PY, Wendum D, Lasnier E, Viallon M, Guéchot J, Hoeffel C, Arrivé L, Tubiana JM, Poupon R. Diffusion-weighted magnetic resonance imaging for the assessment of fibrosis in chronic hepatitis C. *Hepatology* 2007; **46**: 658-665 [PMID: 17663420 DOI: 10.1002/hep.21747]

42 **Wang QB**, Zhu H, Liu HL, Zhang B. Performance of magnetic resonance elastography and diffusion-weighted imaging for the staging of hepatic fibrosis: A meta-analysis. *Hepatology* 2012; **56**: 239-247 [PMID: 22278368 DOI: 10.1002/hep.25610]

43 **Feier D**, Balassy C, Bastati N, Fragner R, Wrba F, Ba-Ssalamah A. The diagnostic efficacy of quantitative liver MR imaging with diffusion-weighted, SWI, and hepato-specific contrast-enhanced sequences in staging liver fibrosis--a multiparametric approach. *Eur Radiol* 2016; **26**: 539-546 [PMID: 25991488 DOI: 10.1007/s00330-015-3830-0]

44 **Wang Y**, Ganger DR, Levitsky J, Sternick LA, McCarthy RJ, Chen ZE, Fasanati CW, Bolster B, Shah S, Zuehlsdorff S, Omary RA, Ehman RL, Miller FH. Assessment of chronic hepatitis and fibrosis: comparison of MR elastography and diffusion-weighted imaging. *AJR Am J Roentgenol* 2011; **196**: 553-561 [PMID: 21343496 DOI: 10.2214/AJR.10.4580]

45 **Ichikawa S**, Motosugi U, Morisaka H, Sano K, Ichikawa T, Enomoto N, Matsuda M, Fujii H, Onishi H. MRI-based staging of hepatic fibrosis: Comparison of intravoxel incoherent motion diffusion-weighted imaging with magnetic resonance elastography. *J Magn Reson Imaging* 2015; **42**: 204-210 [PMID: 25223820 DOI: 10.1002/jmri.24760]

46 **Do RK**, Chandarana H, Felker E, Hajdu CH, Babb JS, Kim D, Taouli B. Diagnosis of liver fibrosis and cirrhosis with diffusion-weighted imaging: value of normalized apparent diffusion coefficient using the spleen as reference organ. *AJR Am J Roentgenol* 2010; **195**: 671-676 [PMID: 20729445 DOI: 10.2214/AJR.09.3448]

47 **Wu CH**, Ho MC, Jeng YM, Liang PC, Hu RH, Lai HS, Shih TT. Assessing hepatic fibrosis: comparing the intravoxel incoherent motion in MRI with acoustic radiation force impulse imaging in US. *Eur Radiol* 2015; **25**: 3552-3559 [PMID: 25991478 DOI: 10.1007/s00330-015-3774-4]

48 **Chung SR**, Lee SS, Kim N, Yu ES, Kim E, Kühn B, Kim IS. Intravoxel incoherent motion MRI for liver fibrosis assessment: a pilot study. *Acta Radiol* 2015; **56**: 1428-1436 [PMID: 25414372 DOI: 10.1177/0284185114559763]

49 **Patel J**, Sigmund EE, Rusinek H, Oei M, Babb JS, Taouli B. Diagnosis of cirrhosis with intravoxel incoherent motion diffusion MRI and dynamic contrast-enhanced MRI alone and in combination: preliminary experience. *J Magn Reson Imaging* 2010; **31**: 589-600 [PMID: 20187201 DOI: 10.1002/jmri.22081]

50 **Girometti R**, Furlan A, Esposito G, Bazzocchi M, Como G, Soldano F, Isola M, Toniutto P, Zuiani C. Relevance of b-values in evaluating liver fibrosis: a study in healthy and cirrhotic subjects using two single-shot spin-echo echo-planar diffusion-weighted sequences. *J Magn Reson Imaging* 2008; **28**: 411-419 [PMID: 18666139 DOI: 10.1002/jmri.21461]

51 **Murphy P**, Hooker J, Ang B, Wolfson T, Gamst A, Bydder M, Middleton M, Peterson M, Behling C, Loomba R, Sirlin C. Associations between histologic features of nonalcoholic fatty liver disease (NAFLD) and quantitative diffusion-weighted MRI measurements in adults. *J Magn Reson Imaging* 2015; **41**: 1629-1638 [PMID: 25256692 DOI: 10.1002/jmri.24755]

52 **Hayashi T**, Miyati T, Takahashi J, Fukuzawa K, Sakai H, Tano M, Saitoh S. Diffusion analysis with triexponential function in liver cirrhosis. *J Magn Reson Imaging* 2013; **38**: 148-153 [PMID: 23239543 DOI: 10.1002/jmri.23966]

53 **Lu PX**, Huang H, Yuan J, Zhao F, Chen ZY, Zhang Q, Ahuja AT, Zhou BP, Wáng YX. Decreases in molecular diffusion, perfusion fraction and perfusion-related diffusion in fibrotic livers: a prospective clinical intravoxel incoherent motion MR imaging study. P*LoS One* 2014; **9**: e113846 [PMID: 25436458 DOI: 10.1371/journal.pone.0113846]

54 **Hansmann J**, Hernando D, Reeder SB. Fat confounds the observed apparent diffusion coefficient in patients with hepatic steatosis. *Magn Reson Med* 2013; **69**: 545-552 [PMID: 23161434 DOI: 10.1002/mrm.24535]

55 **Glover GH**. Multipoint Dixon technique for water and fat proton and susceptibility imaging. *J Magn Reson Imaging* 1991; **1**: 521-530 [PMID: 1790376 DOI: 10.1002/jmri.1880010504]

56 **Bydder M**, Yokoo T, Hamilton G, Middleton MS, Chavez AD, Schwimmer JB, Lavine JE, Sirlin CB. Relaxation effects in the quantification of fat using gradient echo imaging. *Magn Reson Imaging* 2008; **26**: 347-359 [PMID: 18093781 DOI: 10.1016/j.mri.2007.08.012]

57 **Lee JT**, Liau J, Murphy P, Schroeder ME, Sirlin CB, Bydder M. Cross-sectional investigation of correlation between hepatic steatosis and IVIM perfusion on MR imaging. *Magn Reson Imaging* 2012; **30**: 572-578 [PMID: 22285877 DOI: 10.1016/j.mri.2011.12.013]

58 **Le Bihan D**, Poupon C, Amadon A, Lethimonnier F. Artifacts and pitfalls in diffusion MRI. *J Magn Reson Imaging* 2006; **24**: 478-488 [PMID: 16897692 DOI: 10.1002/jmri.20683]

59 **Hernando D**, Levin YS, Sirlin CB, Reeder SB. Quantification of liver iron with MRI: state of the art and remaining challenges. *J Magn Reson Imaging* 2014; **40**: 1003-1021 [PMID: 24585403 DOI: 10.1002/jmri.24584]

60 **Queiroz-Andrade M**, Blasbalg R, Ortega CD, Rodstein MA, Baroni RH, Rocha MS, Cerri GG. MR imaging findings of iron overload. *Radiographics* 2009; **29**: 1575-1589 [PMID: 19959509 DOI: 10.1148/rg.296095511]

61 **Metwally MA**, Zein CO, Zein NN. Clinical significance of hepatic iron deposition and serum iron values in patients with chronic hepatitis C infection. *Am J Gastroenterol* 2004; **99**: 286-291 [PMID: 15046219 DOI: 10.1111/j.1572-0241.2004.04049.x]

62 **Price L**, Kowdley KV. The role of iron in the pathophysiology and treatment of chronic hepatitis C. *Can J Gastroenterol* 2009; **23**: 822-828 [PMID: 20011735 DOI: 10.1155/2009/290383]

63 **Beinker NK**, Voigt MD, Arendse M, Smit J, Stander IA, Kirsch RE. Threshold effect of liver iron content on hepatic inflammation and fibrosis in hepatitis B and C. *J Hepatol* 1996; **25**: 633-638 [PMID: 8938538 DOI: 10.1016/S0168-8278(96)80231-5]

64 **Asayama Y**, Yoshimitsu K, Nishihara Y, Irie H, Aishima S, Taketomi A, Honda H. Arterial blood supply of hepatocellular carcinoma and histologic grading: radiologic-pathologic correlation. *AJR Am J Roentgenol* 2008; **190**: W28-W34 [PMID: 18094269 DOI: 10.2214/AJR.07.2117]

65 **Bruegel M**, Gaa J, Waldt S, Woertler K, Holzapfel K, Kiefer B, Rummeny EJ. Diagnosis of hepatic metastasis: comparison of respiration-triggered diffusion-weighted echo-planar MRI and five t2-

weighted turbo spin-echo sequences. *AJR Am J Roentgenol* 2008; **191**: 1421-1429 [PMID: 18941080 DOI: 10.2214/AJR.07.3279]

66 **Yang DM**, Jahng GH, Kim HC, Jin W, Ryu CW, Nam DH, Lee YK, Park SY. The detection and discrimination of malignant and benign focal hepatic lesions: T2 weighted vs diffusion-weighted MRI. *Br J Radiol* 2011; **84**: 319-326 [PMID: 20959371 DOI: 10.1259/bjr/50130643]

67 **Taouli B**, Vilgrain V, Dumont E, Daire JL, Fan B, Menu Y. Evaluation of liver diffusion isotropy and characterization of focal hepatic lesions with two single-shot echo-planar MR imaging sequences: prospective study in 66 patients. *Radiology* 2003; **226**: 71-78 [PMID: 12511671 DOI: 10.1148/radiol.2261011904]

68 **Okada Y**, Ohtomo K, Kiryu S, Sasaki Y. Breath-hold T2-weighted MRI of hepatic tumors: value of echo planar imaging with diffusion-sensitizing gradient. *J Comput Assist Tomogr* 1998; **22**: 364-371 [PMID: 9606375 DOI: 10.1097/00004728-199805000-00005]

69 **Kim YK**, Lee WJ, Park MJ, Kim SH, Rhim H, Choi D. Hypovascular hypointense nodules on hepatobiliary phase gadoxetic acid-enhanced MR images in patients with cirrhosis: potential of DW imaging in predicting progression to hypervascular HCC. *Radiology* 2012; **265**: 104-114 [PMID: 22891358 DOI: 10.1148/radiol.12112649]

70 **Yuan YH**, Xiao EH, Liu JB, He Z, Jin K, Ma C, Xiang J, Xiao JH, Chen WJ. Characteristics and pathological mechanism on magnetic resonance diffusion-weighted imaging after chemoembolization in rabbit liver VX-2 tumor model. *World J Gastroenterol* 2007; **13**: 5699-5706 [PMID: 17963295 DOI: 10.3748/wjg.v13.i43.5699]

71 **Testa ML**, Chojniak R, Sene LS, Damascena AS, Guimarães MD, Szklaruk J, Marchiori E. Is DWI/ADC a useful tool in the characterization of focal hepatic lesions suspected of malignancy? *PLoS One* 2014; **9**: e101944 [PMID: 25025151 DOI: 10.1371/journal.pone.0101944]

72 **Bruegel M**, Holzapfel K, Gaa J, Woertler K, Waldt S, Kiefer B, Stemmer A, Ganter C, Rummeny EJ. Characterization of focal liver lesions by ADC measurements using a respiratory triggered diffusion-weighted single-shot echo-planar MR imaging technique. *Eur Radiol* 2008; **18**: 477-485 [PMID: 17960390 DOI: 10.1007/s00330-007-0785-9]

73 **Miller FH**, Hammond N, Siddiqi AJ, Shroff S, Khatri G, Wang Y, Merrick LB, Nikolaidis P. Utility of diffusion-weighted MRI in distinguishing benign and malignant hepatic lesions. *J Magn Reson Imaging* 2010; **32**: 138-147 [PMID: 20578020 DOI: 10.1002/jmri.22235]

74 **Heverhagen JT**. Noise measurement and estimation in MR imaging experiments. *Radiology* 2007; **245**: 638-639 [PMID: 18024445 DOI: 10.1148/radiol.2453062151]

75 **Nishie A**, Tajima T, Asayama Y, Ishigami K, Kakihara D, Nakayama T, Takayama Y, Okamoto D, Fujita N, Taketomi A, Yoshimitsu K, Honda H. Diagnostic performance of apparent diffusion coefficient for predicting histological grade of hepatocellular carcinoma. *Eur J Radiol* 2011; **80**: e29-e33 [PMID: 20619566 DOI: 10.1016/j.ejrad.2010.06.019]

76 **Nakajima Y**, Shimamura T, Kamiyama T, Kimura J, Sato N, Matsushita M, Une Y, Uchino J. Evaluation of surgical resection for small hepatocellular carcinomas. *Am J Surg* 1996; **171**: 360-363 [PMID: 8615473 DOI: 10.1016/S0002-9610(97)89642-0]

77 **Heo SH**, Jeong YY, Shin SS, Kim JW, Lim HS, Lee JH, Koh YS, Cho CK, Kang HK. Apparent diffusion coefficient value of diffusion-weighted imaging for hepatocellular carcinoma: correlation with the histologic differentiation and the expression of vascular endothelial growth factor. *Korean J Radiol* 2010; **11**: 295-303 [PMID: 20461183 DOI: 10.3348/kjr.2010.11.3.295]

78 **Woo S**, Lee JM, Yoon JH, Joo I, Han JK, Choi BI. Intravoxel incoherent motion diffusion-weighted MR imaging of hepatocellular carcinoma: correlation with enhancement degree and histologic grade. *Radiology* 2014; **270**: 758-767 [PMID: 24475811 DOI: 10.1148/radiol.13130444]

79 **Guo W**, Zhao S, Yang Y, Shao G. Histological grade of hepatocellular carcinoma predicted by quantitative diffusion-weighted imaging. *Int J Clin Exp Med* 2015; **8**: 4164-4169 [PMID: 26064326]

80 **Nakanishi M**, Chuma M, Hige S, Omatsu T, Yokoo H, Nakanishi K, Kamiyama T, Kubota K, Haga H, Matsuno Y, Onodera Y, Kato M, Asaka M. Relationship between diffusion-weighted magnetic resonance imaging and histological tumor grading of hepatocellular carcinoma. *Ann Surg Oncol* 2012; **19**: 1302-1309 [PMID: 21927976 DOI: 10.1245/s10434-011-2066-8]

81 **Chen CY**, Li CW, Kuo YT, Jaw TS, Wu DK, Jao JC, Hsu JS, Liu GC. Early response of hepatocellular carcinoma to transcatheter arterial chemoembolization: choline levels and MR diffusion constants--initial experience. *Radiology* 2006; **239**: 448-456 [PMID: 16569781 DOI: 10.1148/radiol.2392042202]

82 **Kokabi N**, Camacho JC, Xing M, Edalat F, Mittal PK, Kim HS. Immediate post-doxorubicin drug-eluting beads chemoembolization Mr Apparent diffusion coefficient quantification predicts response in unresectable hepatocellular carcinoma: A pilot study. *J Magn Reson Imaging* 2015; **42**: 981-989 [PMID: 25683022 DOI: 10.1002/jmri.24845]

83 **Park YS**, Lee CH, Kim JH, Kim IS, Kiefer B, Seo TS, Kim KA, Park CM. Using intravoxel incoherent motion (IVIM) MR imaging to predict lipiodol uptake in patients with hepatocellular carcinoma following transcatheter arterial chemoembolization: a preliminary result. *Magn Reson Imaging* 2014; **32**: 638-646 [PMID: 24703575 DOI: 10.1016/j.mri.2014.03.003]

84 **Goshima S**, Kanematsu M, Noda Y, Kondo H, Watanabe H, Bae KT. Diffusion kurtosis imaging to assess response to treatment in hypervascular hepatocellular carcinoma. *AJR Am J Roentgenol* 2015; **204**: W543-W549 [PMID: 25905960 DOI: 10.2214/AJR.14.13235]

85 **Koh DM**, Scurr E, Collins D, Kanber B, Norman A, Leach MO, Husband JE. Predicting response of colorectal hepatic metastasis: value of pretreatment apparent diffusion coefficients. *AJR Am J Roentgenol* 2007; **188**: 1001-1008 [PMID: 17377036 DOI: 10.2214/AJR.06.0601]

86 **Cui Y**, Zhang XP, Sun YS, Tang L, Shen L. Apparent diffusion coefficient: potential imaging biomarker for prediction and early detection of response to chemotherapy in hepatic metastases. *Radiology* 2008; **248**: 894-900 [PMID: 18710982 DOI: 10.1148/radiol.2483071407]

87 **Liang HY**, Huang YQ, Yang ZX, Ying-Ding MS, Rao SX. Potential of MR histogram analyses for prediction of response to chemotherapy in patients with colorectal hepatic metastases. *Eur Radiol* 2016; **26**: 2009-2018 [PMID: 26494642 DOI: 10.1007/s00330-015-4043-2]

88 **Shirota N**, Saito K, Sugimoto K, Takara K, Moriyasu F, Tokuuye K. Intravoxel incoherent motion MRI as a biomarker of sorafenib treatment for advanced hepatocellular carcinoma: a pilot study. *Cancer Imaging* 2016; **16**: 1 [PMID: 26822946 DOI: 10.1186/s40644-016-0059-3]

89 **Lewin M**, Fartoux L, Vignaud A, Arrivé L, Menu Y, Rosmorduc O. The diffusion-weighted imaging perfusion fraction f is a potential marker of sorafenib treatment in advanced hepatocellular carcinoma: a pilot study. *Eur Radiol* 2011; **21**: 281-290 [PMID: 20683597 DOI: 10.1007/s00330-010-1914-4]

90 **Takeda H**, Nishikawa H, Osaki Y, Tsuchiya K, Joko K, Ogawa C, Taniguchi H, Orito E, Uchida Y, Izumi N. Clinical features associated with radiological response to sorafenib in unresectable hepatocellular carcinoma: a large multicenter study in Japan. *Liver Int* 2015; **35**: 1581-1589 [PMID: 24836552 DOI: 10.1111/liv.12591]

91 **Cece H**, Ercan A, Yıldız S, Karakas E, Karakas O, Boyacı FN, Aydogan T, Karakas EY, Cullu N, Ulas T. The use of DWI to assess spleen and liver quantitative ADC changes in the detection of liver fibrosis stages in chronic viral hepatitis. *Eur J Radiol* 2013; **82**: e307-e312 [PMID: 23518145 DOI: 10.1016/j.ejrad.2013.02.022]

92 **Taouli B**, Tolia AJ, Losada M, Babb JS, Chan ES, Bannan MA, Tobias H. Diffusion-weighted MRI for quantification of liver fibrosis: preliminary experience. *AJR Am J Roentgenol* 2007; **189**: 799-806 [PMID: 17885048 DOI: 10.2214/AJR.07.2086]

93 **Kocakoc E**, Bakan AA, Poyrazoglu OK, Dagli AF, Gul Y, Cicekci M, Bahcecioglu IH. Assessment of Liver Fibrosis with Diffusion-Weighted Magnetic Resonance Imaging Using Different b-values in Chronic Viral Hepatitis. *Med Princ Pract* 2015; **24**: 522-526 [PMID: 26183515 DOI: 10.1159/000434682]

94 **Ding Y**, Rao SX, Zhu T, Chen CZ, Li RC, Zeng MS. Liver fibrosis

staging using T1 mapping on gadoxetic acid-enhanced MRI compared with DW imaging. *Clin Radiol* 2015; **70**: 1096-1103 [PMID: 26164421 DOI: 10.1016/j.crad.2015.04.014]

95 **Fujimoto K**, Tonan T, Azuma S, Kage M, Nakashima O, Johkoh T, Hayabuchi N, Okuda K, Kawaguchi T, Sata M, Qayyum A. Evaluation of the mean and entropy of apparent diffusion coefficient values in chronic hepatitis C: correlation with pathologic fibrosis stage and inflammatory activity grade. *Radiology* 2011; **258**: 739-748 [PMID: 21248235 DOI: 10.1148/radiol.10100853]

96 **Bonekamp D**, Bonekamp S, Ou HY, Torbenson MS, Corona-Villalobos CP, Mezey E, Kamel IR. Assessing liver fibrosis: comparison of arterial enhancement fraction and diffusion-weighted imaging. *J Magn Reson Imaging* 2014; **40**: 1137-1146 [PMID: 24989329 DOI: 10.1002/jmri.24472]

97 **Kim YK**, Lee MW, Lee WJ, Kim SH, Rhim H, Lim JH, Choi D, Kim YS, Jang KM, Lee SJ, Lim HK. Diagnostic accuracy and sensitivity of diffusion-weighted and of gadoxetic acid-enhanced 3-T MR imaging alone or in combination in the detection of small liver metastasis (≤ 1.5 cm in diameter). *Invest Radiol* 2012; **47**: 159-166 [PMID: 22330426 DOI: 10.1097/RLI.0b013e31823a1495]

98 **Chung WS**, Kim MJ, Chung YE, Kim YE, Park MS, Choi JY, Kim KW. Comparison of gadoxetic acid-enhanced dynamic imaging and diffusion-weighted imaging for the preoperative evaluation of colorectal liver metastases. *J Magn Reson Imaging* 2011; **34**: 345-353 [PMID: 21702068 DOI: 10.1002/jmri.22671]

99 **Koh DM**, Collins DJ, Wallace T, Chau I, Riddell AM. Combining diffusion-weighted MRI with Gd-EOB-DTPA-enhanced MRI improves the detection of colorectal liver metastases. *Br J Radiol* 2012; **85**: 980-989 [PMID: 22167501 DOI: 10.1259/bjr/91771639]

100 **Löwenthal D**, Zeile M, Lim WY, Wybranski C, Fischbach F, Wieners G, Pech M, Kropf S, Ricke J, Dudeck O. Detection and characterisation of focal liver lesions in colorectal carcinoma patients: comparison of diffusion-weighted and Gd-EOB-DTPA enhanced MR imaging. *Eur Radiol* 2011; **21**: 832-840 [PMID: 20886339 DOI: 10.1007/s00330-010-1977-2]

101 **Shimada K**, Isoda H, Hirokawa Y, Arizono S, Shibata T, Togashi K. Comparison of gadolinium-EOB-DTPA-enhanced and diffusion-weighted liver MRI for detection of small hepatic metastases. *Eur Radiol* 2010; **20**: 2690-2698 [PMID: 20563726 DOI: 10.1007/s00330-010-1842-3]

102 **Donati OF**, Fischer MA, Chuck N, Hunziker R, Weishaupt D, Reiner CS. Accuracy and confidence of Gd-EOB-DTPA enhanced MRI and diffusion-weighted imaging alone and in combination for the diagnosis of liver metastases. *Eur J Radiol* 2013; **82**: 822-828 [PMID: 23287713 DOI: 10.1016/j.ejrad.2012.12.005]

103 **Kim YK**, Kim CS, Han YM, Lee YH. Detection of liver malignancy with gadoxetic acid-enhanced MRI: is addition of diffusion-weighted MRI beneficial? *Clin Radiol* 2011; **66**: 489-496 [PMID: 21367403 DOI: 10.1016/j.crad.2010.09.007]

104 **Goshima S**, Kanematsu M, Kondo H, Yokoyama R, Kajita K, Tsuge Y, Watanabe H, Shiratori Y, Onozuka M, Moriyama N. Diffusion-weighted imaging of the liver: optimizing b value for the detection and characterization of benign and malignant hepatic lesions. *J Magn Reson Imaging* 2008; **28**: 691-697 [PMID: 18777553 DOI: 10.1002/jmri.21467]

105 **Battal B**, Kocaoglu M, Akgun V, Karademir I, Deveci S, Guvenc I, Bulakbasi N. Diffusion-weighted imaging in the characterization of focal liver lesions: efficacy of visual assessment. *J Comput Assist Tomogr* 2011; **35**: 326-331 [PMID: 21586924 DOI: 10.1097/RCT.0b013e318216efeb]

106 **Gourtsoyianni S**, Papanikolaou N, Yarmenitis S, Maris T, Karantanas A, Gourtsoyiannis N. Respiratory gated diffusion-weighted imaging of the liver: value of apparent diffusion coefficient measurements in the differentiation between most commonly encountered benign and malignant focal liver lesions. *Eur Radiol* 2008; **18**: 486-492 [PMID: 17994317 DOI: 10.1007/s00330-007-0798-4]

107 **Namimoto T**, Yamashita Y, Sumi S, Tang Y, Takahashi M. Focal liver masses: characterization with diffusion-weighted echo-planar MR imaging. *Radiology* 1997; **204**: 739-744 [PMID: 9280252 DOI: 10.1148/radiology.204.3.9280252]

108 **Kim T**, Murakami T, Takahashi S, Hori M, Tsuda K, Nakamura H. Diffusion-weighted single-shot echoplanar MR imaging for liver disease. *AJR Am J Roentgenol* 1999; **173**: 393-398 [PMID: 10430143 DOI: 10.2214/ajr.173.2.10430143]

109 **Cieszanowski A**, Anysz-Grodzicka A, Szeszkowski W, Kaczynski B, Maj E, Gornicka B, Grodzicki M, Grudzinski IP, Stadnik A, Krawczyk M, Rowinski O. Characterization of focal liver lesions using quantitative techniques: comparison of apparent diffusion coefficient values and T2 relaxation times. *Eur Radiol* 2012; **22**: 2514-2524 [PMID: 22699872 DOI: 10.1007/s00330-012-2519-x]

110 **Demir OI**, Obuz F, Sağol O, Dicle O. Contribution of diffusion-weighted MRI to the differential diagnosis of hepatic masses. *Diagn Interv Radiol* 2007; **13**: 81-86 [PMID: 17562512]

111 **Oner AY**, Celik H, Oktar SO, Tali T. Single breath-hold diffusion-weighted MRI of the liver with parallel imaging: initial experience. *Clin Radiol* 2006; **61**: 959-965 [PMID: 17018309 DOI: 10.1016/j.crad.2006.06.014]

112 **Holzapfel K**, Bruegel M, Eiber M, Ganter C, Schuster T, Heinrich P, Rummeny EJ, Gaa J. Characterization of small (≤10 mm) focal liver lesions: value of respiratory-triggered echo-planar diffusion-weighted MR imaging. *Eur J Radiol* 2010; **76**: 89-95 [PMID: 19501995 DOI: 10.1016/j.ejrad.2009.05.014]

113 **Saito K**, Moriyasu F, Sugimoto K, Nishio R, Saguchi T, Akata S, Tokuuye K. Histological grade of differentiation of hepatocellular carcinoma: comparison of the efficacy of diffusion-weighted MRI with T2-weighted imaging and angiography-assisted CT. *J Med Imaging Radiat Oncol* 2012; **56**: 261-269 [PMID: 22697322 DOI: 10.1111/j.1754-9485.2012.02374.x]

114 **Nasu K**, Kuroki Y, Tsukamoto T, Nakajima H, Mori K, Minami M. Diffusion-weighted imaging of surgically resected hepatocellular carcinoma: imaging characteristics and relationship among signal intensity, apparent diffusion coefficient, and histopathologic grade. *AJR Am J Roentgenol* 2009; **193**: 438-444 [PMID: 19620441 DOI: 10.2214/AJR.08.1424]

P- Reviewer: Bubnov RV, Ferraioli G, Gatselis NK, Waisberg J
S- Editor: Kong JX **L- Editor**: A **E- Editor**: Lu YJ

Published by **Baishideng Publishing Group Inc**
8226 Regency Drive, Pleasanton, CA 94588, USA
Telephone: +1-925-223-8242
Fax: +1-925-223-8243
E-mail: bpgoffice@wjgnet.com
Help Desk: http://www.wjgnet.com/esps/helpdesk.aspx
http://www.wjgnet.com